Journal of Basic and Environmental Sciences 1 (2014) 46 - 64 ISSN 2356-6388

Thermal Decomposition of Metal Tartrates through the Prepration of Nano Cobalt Ferrite

M. Sameeh, M. Khairy, W. A. Bayoumy,Tomader El-asawi, A.A. El-bellihi

Chemistry department, faculty of science, Benha University, Benha, Egypt.
*Corresponding author. E-mail: marwa_sameeh@yahoo.com

Article Information

Received; 1 October. 2013
In Revised form; 30 October, 2013
Accepted; 30 October, 2013

Keywords:
Nano $CoFe_2O_4$
Spine
Tartrate salts
Thermal kinetics
Eelectrical conductivity

Abstract

Nano-crystalline $CoFe_2O_4$ particles were synthesized through thermal decomposition of cobalt tartrate- ferric tartrate at 250, 450, 750 and 1050°C. The samples were characterized by XRD, DSC-TG, SEM, TEM and FT-IR. The XRD analysis showed that the sample calcined at 1050 °C exhibit pure spinel phase. The crystallite sizes lie in the range of 30 – 61 nm. The samples obtained at different calcination temperatures have different morphologies. The kinetics of thermal decomposition of metal tartrate mixtures were studied using non-isothermal thermogravimetric techniques. The thermal decomposition proceeds in three steps for cobalt iron (III) tartrate. The kinetic analysis of non-isothermal data of the decomposition reaction is best described by the Random nucleation in (three-dimentions) (A4) models. The activation parameters were calculated and the results of the dynamic integral methods were compared and discussed.

1. INTRODUCTION

Oxide spinels having the general formula AB_2O_4 [1–3] represent a large class of inorganic materials which possess many useful properties not found in the more limited binary oxides since they exhibit interesting structural, electrical, magnetic and catalytic properties. Their physical properties were found to be dependent on the nature of the ions involved, their charges, and their site distribution.

Nanosized materials exhibit remarkable superior properties to those of bulk materials. These materials are very much interesting because of their size dependent optical, electrical, magnetic, thermal, mechanical and chemical properties. Nano-$CoFe_2O_4$ particle is a hard magnetic material that has a high coercivity; high cubic magneto crystalline anisotropy, excellent chemical stability and mechanical hardness. By considering all these properties cobalt ferrite is a promising material for many applica- tions such as gas sensors, microwave devises ,magnetic resonance imaging, magnetic fluids, spintronics, solar cells, high density and magnetic properties of cobalt ferrites get differ due to the presence of cobalt ions in the tetrahedral sites coupled with various oxidation states of cobalt ions [4] The electrical properties exhibited by ferrites in the micron region are normally characteristic of hoping of electrons or holes or polarons between cationic sites. Thus the cation distributions as well as oxidation states of the cations also determine the dielectric polarization and electrical conduction [5, 6]. In order to understand the oxidation state and spin related phenomenon the EPR spectroscopy will give valuable information [7]. Various preparation procedures such as, sol–gel, citrate precursor, electro chemical, combustion, solid state reaction and mechanical alloying methods are used to get

ready ferrite nanoparticle [8, 9, 10]. Several techniques have been employed to synthesize this material at the nanoscale. These methods include sol–gel [11, 12)], micelle chemical control method (micro-emulsion) [13], citrate-gel method [14, 15], hydrothermal process [16], polymerized complex method [17], mechanical alloying [14, 18, 19], mechanochmical method [20], and electrospinning [21]

Thermal decomposition as a solid state process is important technique which offers many possibilities for chemical structure modifications, as well as in the preparation of new materials at the nanoscale [22]. The kinetics of the thermal decomposition steps in air can be studied by using isothermal and non-isothermal thermo-gravimetric techniques. Various reaction interface models and different techniques of computational analysis of non-isothermal data were used to discuss the results. The activation parameters, calculated by using a composite method of integral analysis of non-isothermal data, revealed not only their independence from the heating rate and fractional reaction, but also a better correlation and agreement with the results obtained under isothermal conditions.

In the present study, $CoFe_2O_4$ spinel was prepared through thermal decomposition of cobalt tartrate- iron(III) tartarate with (1:1) mole fraction. The thermal decomposition behavior was investigated using DTA-TG, SEM and TEM techniques. The electrical properties (conductivity, dielectrical constant and dielectric loss) for the prepared spinel were studied. The crystal structure and the change in morphology through thermal treatment were studied by XRD, FT-IR, SEM and TEM. The kinetics of the decomposition steps were investigated by non-isothermal thermogravimetric techniques using various reaction interface models.

2. EXPERIMENTAL

2.1. Materials

All chemicals were analytical grade and used as purchased without further purification. Tartaric acid ($C_4H_6O_6$) (99%) Supplied by Mallinkrodt, INC, ferric nitrate (Fe $(No_3)_3.9H_2O$) (99%) by BDH, cobalt carbonate ($Co(Co_3).Co(OH)_2$) (99%) by Mallin ckordt and ethyl alcohol (Seoul, 99.5%). Distilled water was used throughout the whole experiments.

2.2. Synthesis of metal tartrates

2.2.1. Preparation of $CoC_4H_4O_6$

$CoC_4H_4O_6$ was prepared by adding basic $Co(Co_3).Co(OH)_2$ to hot solution of tartaric acid. The solution was stirred vigorously in a water bath until a solid product was obtained. The precipitate was filtered then washed several times with distilled water. Then it dried at $80^{O}C$ for two hrs.

2.2.2. Preparation of $FeC_4H_4O_6$

Two solutions were prepared for this process: (i) tartaric acid ($C_4H_6O_6$) was dissolved in ethyl alcohol to produce a tartaric acid solution, and ferric nitrate (Fe $(No_3)_3.9H_2O$), was dissolved in ethyl alcohol and then stirred at room temperature until the solution became transparent. The cation solution was then added to the tartaric acid solution. The resulting solution precipitated at room temperature over the course of 1 h as it was stirred constantly to ensure the completion of the complex reactions. The solution was then dried at 80 ◦C for24 h.

2.3. Synthesis of $CoFe_2O_4$

$CoC_4H_4O_6$ - $FeC_4H_4O_6$ were prepared by the impregnation of $CoC_4H_4O_6$ with $FeC_4H_4O_6$ in molar ratio of (1:1) Co: Fe. This mixture was heated at different temperature as 250, 450, 750 and 1050 ^{o}C for 4hrs. The samples prepared were denoted as $CoFe_{250}$, $CoFe_{450}$, $CoFe_{750}$, $CoFe_{1050}$, respectively.

2.4. Kinetic Consideration

In general, the rate constant, K of a solid-state reaction is given by the formal kinetic equation:

$$\frac{d\alpha}{dt} = Kf(\alpha) = Ae^{-E/RT} f(\alpha) \qquad (1)$$

Where α is the fractional reaction; t, is time; A is the pre-exponential factor; E is the activation energy; R is the gas constant; T is temperature in Kelvin, and $f(\alpha)$ is the kinetic function, which takes different forms depending on the particular reaction rate equation [23-25]. In isothermal kinetic studies, the rate equation used to calculation the rate constant has the form

$$g(\alpha)=kt \qquad (2)$$

Where $g(\alpha)=\int_0^{\alpha} \frac{d\alpha}{f(\alpha)}$ is the integrated from of $f(\alpha)$[23-25]. However, non-isothermal methods are becoming more widely used because they are more convenient than the classical isothermal methods [26].

In non-isothermal kinetics, the time dependence on the left side of Eq. (1) is eliminated by using a constant heating rate $\beta=dT/dt$, so that $T=T_o+\beta$ where T_o is the starting temperature and t is the time of heating. With the use of integral method of analysis, Eq. (1) may be written as

$$g(\alpha)=\frac{A}{\beta}\int_{T_o}^{T} e^{-E/RT}\, dt \qquad (3)$$

The reaction rate is negligible at low temperature. Hence: $g(\alpha)=\frac{A}{\beta}\int_0^T e^{-E/RT} dt$ (4)

Integration of this equation leads to Doyle's equation [27]:

$$g(\alpha)=\frac{AE}{R\beta}\left[\frac{e^{-x}}{x} - \int_0^{\infty}\frac{e^{-u}}{u}du\right] = \frac{AE}{R\beta}P(x) \qquad (5)$$

Where $u = E/RT$ and x is the corresponding value of u at which a fraction of material has decomposed. This equation has been reformulated [28] as:

$$\ln g(\beta) - \ln P(x) = \ln\frac{AE}{R\beta} = B \qquad (6)$$

Where B is a constant for a particular reaction at a constant heating rate β. The integral function P(X) is not definite; it may be written in an expanded from and estimated by using a procedure of trial-error type involving iteration [29].

In the present study, analysis of non-isothermal data was performed by using the approximate computational approaches due to Coats and Redfern [30], Ozawa [31], Mahusudanan [32] and Diefallah [33]. Integral methods are often more reliable and generally preferred than differential method of kinetic analysis.

In the Coats-Redfern method [30], the function $g(x)$ is approximated to the form

$$g(\alpha) = \frac{ART^2}{\beta E}\left[1 - \frac{2RT}{E}\right]e^{-E/RT} \qquad (7)$$

The equation has been written in the form:

$$-\ln[\frac{g(\alpha)}{T^2}] = \ln\frac{AR}{\beta E}\left(1-\frac{2RT}{E}\right)+\frac{E}{RT} \qquad (8)$$

The quantity ln$[(AR)/(\beta E)](1-2RT/E)$ is reasonably constant for most values of E and in the temperature range over which most reaction occure. However, both E and A could vary with the experimental heating rate.

In the Ozawa method [31], a master curve has been derived from the TG data obtained at different heating rates (β) by using Doyle's equation and assuming that [AE/β]P(E/RT) is a constant for given function of material decomposed. The function p(E/RT) was approximated by the equation:

$$LogP(\frac{E}{RT}) = -2.315 - 0.4567(\frac{E}{RT}) \qquad (9)$$

So that

$$-log\beta = 0.4567\left(\frac{E}{RT}\right) + constant \qquad (10)$$

Hence, the activation energy is calculated from thermo gravimetric data obtained at different heating rates. The frequency factor is calculated from the equation

$$log\ A = log\ g(\alpha) - log\ [\frac{E}{\beta R}P\frac{E}{RT}] \qquad (11)$$

Although the calculation activation energy is independent of the reaction model, and the frequency factor depends on the determined from of g(x), both E and A could vary considerably with the fractional reaction [23].

In the Madhusudannan method [32], the equation used has the form:

$$-ln\left[\frac{g(\alpha)}{T^{1.921503}}\right] = -ln\frac{AR}{\beta E} + 3.7720501 - 1.921503lnE - \frac{E}{RT} \qquad (12)$$

Where the symbols have their usual significance. The activation energy E and the frequency factor A are obtained from the slope and intercept of the linear fit of the plot of $-ln[g(\alpha)/T1.921503]\ vs.\ 1/T$.

In the composite method of analysis of dynamic data [23], the result obtained (not only at different heating rates, but also at different α values) are superimposed on one master curve. This was achieved by rewriting the approximate integral equations due to different workers in the form such that the kinetic function g(α) and the linear heating rate β lie on one side of equation and 1/T on the other side. When use is made of the modified Coats-redfern equation [30], then in order to allow the composite analysis equation is written in form

$$ln\left[\frac{\beta g(\alpha)}{T^2}\right] = ln\left(\frac{AR}{E}\right) - \frac{E}{RT} \qquad (13)$$

Hence, the dependence of $ln\left[\frac{\beta g(\alpha)}{T^2}\right]$ calculated for different α values at their respective β values on 1/T must give rise to single master straight line for correct form of g(α) , and a single activation energy and frequency factor can readily be calculated.

When Doyle's approximate equation [27] is used, the equation for composite analysis has the form

$$\log[\beta\, g(\alpha)]=[\log\frac{AE}{R}-2315]-0.4567\frac{E}{RT} \qquad (14)$$

Use may also be made of the approximate equation [32] of Madhusudanan, rewritten as

$$-\ln[\frac{\beta g(\alpha)}{T^{1.921503}}]=-\ln\frac{AR}{E}+3.7720501-1.9211503\ln E-\frac{E}{RT} \qquad (15)$$

Again, the dependence of the left side Eqs (14) and (15) on hence the activation energy and the frequency factor can readily be calculate.

In general, the use of different approximate integral equations for kinetic analysis of non-isothermal decomposition kinetic data according to the composite method of analysis gave rise, within experimental error, to identical values of the activation parameters and the correct form of g(α). A computer program has been written to perform the data analysis [33].

3- RESULTS AND DISCUSSION

3-1. X-ray diffraction (XRD)

Powder XRD analysis was used to examine the crystal structure of the samples. The XRD patterns of the Cobalt - iron tartrate mixture calcined at 250, 450, 750 and 1050 °C are shown in Fig. 1. As shown in Fig. 1a, the XRD patterns of sample calcined at 250 ◦C show diffraction peaks indicated the presence of Cobalt tartrate phase and iron oxide. XRD patterns of sample calcined at 450 ◦C (Fig. 1b), show the formation of γ-Fe_2O_3 and Co_3O_4 indicating the absence of spinel crystal structure.For the sample calcined at 750 ◦C (Fig. 1c), XRD lines show the presence of $CoFe_2O_4$,CoO and Fe_2O_3. On further heating to 1050 ◦C (Fig. 1d), only XRD lines characteristic $CoFe_2O_4$ spinel.

Spinel structure of $CoFe_2O_4$ was formed this on the basis of diffraction peaks corresponding to Miller indices of (220) and (311) which confirms the formation of a cubic spinel structure (Table 1). The results obtained by X-ray diffraction patterns were indexed using the standard JCPDS card no. 22-1086 [34].

The absence of any XRD pattern for other metal oxides is referring to complete interactions between the reactant materials. The intensity of the diffraction peaks increases with increasing calcination temperature, which is associated with an increase in the crystallinity.

The average crystallite size D was evaluated using the Scherrer's formula [35], $D = 0.9\lambda/\beta\cos\theta$, where λ is the wavelength of Cu K_α radiation, θ is the Bragg diffraction angle of the line and β is the full- width at half-maxima (FWHM) of XRD peaks. In our experiment, β was corrected by this formula: $\beta = \beta_m - \beta_S$, Where β_m is the measured FWHM of the sample studied, β_S the FWHM of silica, which was used to avoid the broadening from the X-ray instrument. The average crystallite sizes obtained for all samples lie in the range of 30 – 61 nm. It was observed that the crystallite size increases with increasing the calcinations temperatures, Table 1.

3-2. SEM analysis

SEM images of the Cobalt-iron tartrate mixture calcined at 250, 450, 750 and 1050 ˚C are shown in Fig. 2. Inspections of the images show the formation of different aggregated of small particles, homogeneous as shape and size. The sample heated at 250 ˚C shows particle with large aggregate while by increasing the temperature to 450 ˚C shows plate structure, but the sample at 750 the morphology changed to aggregated sheets structure while at 1050 ˚C shows fibers-plate structure. This change in the morphologies of samples may be attributed to the calcinations temperature which attributed to different compositions.

TEM images of the nano-sized Cobalt-iron tartrate mixture calcined at 250, 450, 750 and 1050 ˚C are shown in Fig. 3. It shows particle with different morphologies. The sample heated at 250 ˚C shows particle with large aggregate with particle size 46 nm while by increasing the temperature to 450 ˚C shows plate structure with particle size 15 nm , but the sample at 750 the morphology changed to aggregated sheets structure with particle size 111 nm while at 1050 ˚C shows fibers-plate structure with particle size52 nm. The particle size was found to be dependent on the calcination temperature where the particle sizes increases as the temperature increases this may be attributed to the sintering of particles or due to the generation of the oxides form with high crystallinity as confirmed from XRD results.

3-3. FTIR spectroscopy

The FT-IR data of the Cobalt-iron tartrate mixture calcined at 250, 450, 750 and 1050 ˚C are shown in Table 1. The FT-IR absorptions were recorded at room temperature in the wavenumber range 200–1000cm^{-1}. In the range 1000–200cm^{-1}, the IR bands of solids are usually assigned to vibration of ions in the crystal lattice. According to Waldron [36], ferrites can be considered continuously bonded crystals, that is the atoms are bonded to all nearest neighbours by equivalent forces (ionic, covalent or van der Waals). In ferrites the metal ions are situated at two different sublattices designated tetrahedral (A-site) and octahedral (B-site) according to the geometrical configuration of the oxygen nearest neighbours. According to Waldron [36] the band ν_1 is attributed to the stretching vibration of Fe^{3+}–O^{2-} in tetrahedral complexes that generally observed in the range 600–550cm^{-1}and ν_2 is assigned to that of bending vibrations in octahedral complexes that usually observed in the range 450–385cm^{-1}. The position and intensities of ν_1 and ν_2 vary slightly due to the difference in the Fe^{3+}–O^{2-} distances for the tetrahedral and octahedral sites.

The FTIR spectra of sample calcined at 750°C shows that the presence of bands characteristics to oxides and spinel structure. And appearing to bands related to OH asymmetric and water adsorbed on the surface of oxides. The spinel crystal structure of $CoFe_2O_4$ that appeared after calcinations at 1050 ^{o}C can be easily identified by means of two main broad metal–oxygen bands are seen in the IR spectra of all spinels, and ferrites in particular. The two absorption bands at high wave number (579- 458cm^{-1}) are corresponding to vibration of ions of valence Co^{2+} in tetrahedral positions and the band at low frequency (around 437- 422 cm^{-1}) is corresponding to vibration of ions of Fe^{+3} in octahedral sites. Table1.

The analysis of the FTIR spectra of samples show that there is appreciable change in the intensity of the bands (400-750 cm^{-1} region) occurring with the modification in the chemical composition of the samples and the change in the calcinations temperature.

3.4. Thermal analysis:

Figure 5 shows the DSC-TGA curves in air at heating rate 10 deg/min in the temperature range from room temperature to 1050 ^oC for $CoC_4H_4O_6$, $Fe_2(C_4H_4O_6)_3$ and $CoC_4H_4O_6$-$Fe_2(C_4H_4O_6)_3$.$21H_2O$ mixture with (1:1) mole ratio.

3.4.1. Iron (III) tartrate hydrate $Fe_2(C_4H_4O_6)_3.5H_2O$:

The TGA curve (not shown) showed that the decomposition takes place in two steps. The first step begins at 50^oC and completed at 120^oC which characterized by an endothermic peak at 80^oC forming accompanied with a weight loss of about 13.93% (theoretical value 13.56%). This step is attributed to the loss of water of crystallization and formation of anhydrous iron(III) tartrate .The second decomposition step in TGA starts at 200^oC and completed at 290^oC which characterized by an exothermic peak at 270^oC forming accompanied with a weight loss of about 61.96% (theoretical value 65.04%). This step is due to the decomposition of Fe_2 $(C_4H_4O_6)_3$ to Fe_2O_3.

3.4.2. Cobalt tartrate hydrate $CoC_4H_4O_6.9H_2O$:

The TGA curve (not shown) showed that the decomposition takes place in two steps. The first step begins at 150^oC and completed at 220^oC which characterized by an endothermic peak at 180^oC forming accompanied with a weight loss of about 20.68% (theoretical value 19.91%) . This step is attributed to the loss of water of crystallization and formation of anhydrous cobalt tartrate .The second decomposition step in TGA starts at 310^oC and completed at 400^oC which characterized by an exothermic peak at 384^oC forming accompanied with a weight loss of about 50% (theoretical value 51.55%). This step is due to the decomposition of Fe_2 $(C_4H_4O_6)_3$ to Fe_2O_3.

3.4.3. $CoC_4H_4O_6$-$Fe_2(C_4H_4O_6)_3$ mixture:

Figure 5 shows the TGA curve of $CoC_4H_4O_6$-Fe_2 $(C_4H_4O_6)_3$ mixture. The curve showed that the mixture losses weight in four steps. The first step begins at 80^oC and completed at 120^oC which characterized by an endothermic peak at 90^oC forming accompanied with a weight loss of about 14.06% (theoretical value 14.17%). This step is attributed to the loss of water of crystallization and formation of anhydrous $CoC_4H_4O_6$-Fe_2 $(C_4H_4O_6)_3$ mixture. The second decomposition step in TGA starts at 230^oC and completed at 290^oC which characterized by an exothermic peak at 259^oC forming accompanied with a weight loss of about 47.43% (theoretical value 45%). This step is due to the decomposition of Fe_2 $(C_4H_4O_6)_3$ present in mixture to Fe_2O_3. The third decomposition step in TGA starts at 295^oC and completed at 340^oC which characterized by an exothermic peak at 300^oC forming accompanied with a weight loss of about14.88% (theoretical value 13.46%).This step is due to the decomposition of $CoC_4H_4O_6$ present in mixture to Co_3O_4. The fourth decomposition step in TGA starts at 895^oC and completed at 940^oC which characterized by an endothermic peak at 910^oC forming accompanied with aweight loss of about 0.58% (theoretical value0.6%). The remarkable decrease in the decomposition temperature of the metal tartrate mixtures, from 384 ^{o} C to 270° C, could be attributed to the formation of the single phase product. It is also evident that the TGA traces of the intimately mixed powders do not reveal intermediate curve breaks either at the fast or at the slow heating rates. XRD proves that cobalt ferrite formation start at 300 ^{o} C. Diefallah et al. [37-39] pointed out that the particle size ratio of $BaCO_3$ TO TiO_2 in the reaction mixture is closely related to the formation of intermediate phases. It was suggested that the reaction between BaCO3 and coarse TiO_2 to form $BaTiO_3$ proceeds in three steps with the formation of Ba_2TiO_4 during the reaction,whereas in equimolar mixtures of $BaCO_3$-fine TiO_2,the reaction leads directly to $BaTiO_3$.

Figure depicts the fraction reaction remaining as a function of temperature, for the decomposition steps. Kinetic of non-isothermal decomposition of mixed tartrate: $CoC_4H_4O_6$-Fe_2 $(C_4H_4O_6)_3.21H_2O$ mixture with (1:1) mole ratio losses weight in three well defined steps, one for dehydration and the other two steps for the decomposition of anhydrous mixture to Co_3O_4-Fe_2O_3 mixture. The kinetics of these three decomposition steps in air were studied under non-isothermal conditions at heating rates 5,10,15 and 20 deg min^{-1}. Figure 5 shows representative weight changes (1-α values) as a function of temperature obtained from the dynamic measurements for the thermal decomposition of $CoC_4H_4O_6$-Fe_2 $(C_4H_4O_6)_3.21H_2O$ mixture at different heating rates for the three decomposition stages. The kinetic analysis of these decomposition steps was performed with reference to the different models of heterogeneous solid-state reactions using the Deifallah's composite method of integral kinetic analysis. The results showed that both composite methods of analysis gave equivalent curves and identical values for the activation parameters, and that the dehydration, first decomposition and second decomposition steps were best described by the phase Random nucleation three-dimentions (A4) model.

The results in tables 2 shows that both composite methods of analysis gave indentical values for the activation parameters with less stander deviation and highest correlation coefficient and the results were in agreement with those calculated according to Coats-Redfern and Mudhusudanan method. Ozawa method gives less satisfactory results.

3.5. Electrical properties

3.5.1. Temperature dependence of AC conductivity (σ_{ac})

Fig. 6 shows typical curves correlate the ac conductivity ($\ln\sigma_{ac}$) and the reciprocal of absolute temperature (1000/T) for $CoFe_2O_4$ in the frequency range from 10 Hz to 5MHz. It can be concluded that the conductivity for the sample is frequency slightly dependent at all temperature regions. On the other hand, the conductivity of sample was found to be temperature dependent. The curve shows three regions are obtained by increasing the temperature. In the first region in the range of temperature of 300 to 448 K, the electrical conductivity is changed with temperature which give rise to a metallic behavior at frequencies (<200 kHz) . After that the conductivity was found to increase with increasing temperature giving a kink in each curve which is referring to that the sample behave as semiconductors or insulators and approach a maximum value at about 448 K and then decreases. The conductivity was found to decreases in the range of temperature of 448 to 598 K at all frequencies this indicating the metallic behavior of sample in this range. Then the conductivity values increases again after 589K indicating the semiconducting behavior.

The electrical conductivity-temperature behavior obeys Wilson's law [18].

$\sigma = \sigma_0 \exp[-E/kT]$

σ_0 is the pre-exponential factor, contains several constants, including the vibrational frequency of the potentially mobile ions, *E* the activation energy, *k* is Boltzmann's constant, and *T* is the absolute temperature. The activation energies were calculated for the 1st and 3rd regions, firstly for low-temperature region: E_I and secondly for high-temperature region: E_{II}. The calculated values of the activation energy are listed inTable3. It is interesting to observe that the activation energy in the high-temperature region is higher than that in the low-temperature one. It was found that the conducting is hopping according to the value of power s in the relation $\sigma_{Ac} = A\omega^s$ that is lays in the range 0 and 1.

3.5.1. AC conductivity (σ_{ac}) with frequency

In order to understand the conduction mechanism and the type of polarons responsible for conduction, the variation of ac conductivity (σ_{ac}) as a function of frequency is represented in Fig. 7. It is also well known that, in large polaron hopping, the ac conductivity decreases with frequency whereas in small polaron hopping it increases with frequency

[40,41].The electrical conduction mechanism in terms of the electron and polaron hopping model has been discussed by Austin and Mott [42]. At lower frequencies, the grain boundaries are more active and hence the hopping of Fe^{2+} and Fe^{3+} ions is less at lower frequencies. As the frequency of the applied field increases, the conductive grains become more active, thereby promoting electron hopping between two adjacent octahedral sites (B-sites) in the spinel lattice and a transition between Fe^{2+} and Fe^{3+} ions, thereby increasing the hopping conduction. In the present case, the plots for ac conductivity measurement are linear, indicating that the conduction is due to small polarons. It has been shown that, for ionic solids, the concept of small polaron is valid [43]. Therefore a gradual increase in conductivity was observed with frequency. As reported by Alder and Fienleib [44], the frequency-dependent conduction is mainly attributed to a small polaron-type hopping mechanism.

3.5.2. Dielectric properties

Fig. 8 shows typical curves illustrate the variation of the dielectric constant (ε`) with the absolute temperature as a function of frequency. The dielectric constant was found to decrease with increasing frequency for all the samples which can be considered as a normal dielectric behavior [45, 46]. This decrease was rapid at lower frequencies and slower at higher frequencies. The dielectric structure was supposed to be composed of two layers. The highly conducting grains, which are separated by relatively poor conducting substances called the grain boundaries. This causes the localized accumulation of charges under the influence of electric field, which results in interfacial polarization. At higher frequencies the electron exchange between ferrous and ferric ions cannot follow the alternating field, which causes a decrease in the contribution of interfacial polarization in dielectric constant, and thus a decrease in the dielectric constant obtained. Fig. 8 also shows that, the dielectric constant increases gradually with increasing temperature up to a certain level, with a position depending on the applied frequency, which is designated as the dielectric transition temperature (*T*d). However, beyond this temperature the values of dielectric constant for all the samples were found to decrease continuously. This progressive increase in (ε`) with temperature is due to the large number of dipoles that becomes free with such high thermal energy and the field aligned them in its direction.The decrease of (ε`) is attributed to the decrease in internal viscosity of the system giving rise to more degrees of freedom to the dipoles with the result of increasing the disordering in the system and hence decreasing (ε`) again. The values of T_d were found to be in good agreement with the values of transition temperature(*T*c) observed in Fig. 1 .{($\ln\sigma_{ac}$) vs 1000/T at 448k}.

The variation of dielectric loss for the sample annealed at various temperatures as a function of frequency is shown in Fig. 9. The dielectric loss decreases as the frequency increases. The decrease is rapid at lower frequency region and remains constant at higher frequencies. The decrease takes place when the jumping frequency of electric charge carriers could not follow the alternation of applied ac electric field beyond a certain critical frequency. Dielectric variation in ferrite molecules can be explained on the basis of space charge polarization, which is a result of the presence of higher conductivity phases (grains) in the insulation of matter (grain boundaries) of a dielectric causing localized accumulation of charges under the influence of an electric field. The sample shows variation due to Maxwell Wagner type interfacial polarization in agreement with Koops phenomenological theory. The large value of dielectric constant at lower frequency is attributed to different type of polarizations (electronic, atomic, interfacial, and ionic) and as the frequency increases, ionic and orientation sources of polarizability decreases and finally disappear due to inertia of the molecules and ions. The mechanism of this dielectric polarization may also be attributed to the dipoles resulting from the change in valence of cations, such asFe^{3+}/Fe^{2+}. The polarization at lower frequencies may result from the electron hopping between Fe^{3+}/Fe^{2+} ions in ferrite lattice [47–49]. Fig. shows variation of dielectric loss (ε``) with frequency for the

ferrites, which shows a similar variation as that of the dielectric constant with frequency. The low value of dielectric loss indicates that the synthesized ferrites can be used in high frequency applications.

4. CONCLUSION

Nano cobalt ferrite was synthesized by thermal decomposition method. The influence of calcination temperature on structure and morphology was studied using XRD,TEM, SEM and FT-IR techniques. The tartrate decomposition process was monitored using TGA-DSC techniques. XRD patterns showed the formation the cubic spinel structure at 1050°C. SEM and TEM reveals that the different morphology of the sample depends on calcinations decomposition temperature. The kinetic of decomposition steps were investigated. From TGA curve the decomposition takes place in four steps. The results showed that both composite methods of analysis gave equivalent curves and identical values for the activation parameters and decomposition steps were best described by the phase Random nucleation three-dimension (A4) model. The conductivity data showed semiconducting behavior and refer to a hopping conduction mechanism via electron transfer between valence states of transition metal ions. Dielectric constant depends on frequency and temperature.

REFERENCES

[1] G. Blasse, Energy transfer in oxidic phosphors, Philips Res. Report. 20 (1965) 528.

[2] M. A. Mousa, M. A. Ahmed, Electrical conduction in γ-irradiated and unirradiated zinc-iron ferrites ,Thermochim. Acta.125 (1988) 379.

[3] M. A. Ahmed, E. H. El-Khawas, S. T. Bishay, Comparison studies of electrical and magnetic behavior of Li-Cd ferrite, J. Mater. Sci. Lett.19 (2000) 791.

[4] E. V. Gopalan, P. A. Joy, I. A. Al-Omari, D. S. Kumar, Y. Yoshida, M. R. Anantharaman, On the structural,magnetic and electrical properties of sol-gel derived nanosized cobalt ferrite, J. Alloys Compds. 485 (2009) 711.

[5] P. P. Hankare, U. B. Sankpal, R. P. Patil, P. D. Lokhande, R. Sasikala, Synthesis, characterization and catalytic activity of chromium substituted cobalt ferrospinels, Mater. Sci. Eng. B 176 (2011) 103.

[6] A. Thakur, P. Thakur, J.Hsu, Novel magnetodielectric nanomaterials with matching permeabilityand permittivity for the very-high-frequency applications, Scr. Mater. 64 (2011) 205.

[7] M. Chand, A. Kumar, Annver, S. Kumar, A. Shankar, R. P. Pant, Investigation on $Mn_xZn_{1-x}Fe_2O_4$(x=0.1,0.5) nanoparticles synthesized by sol-gel and co-precipitation methods, Indian J. Eng. Mater. Sci. 18 (2011) 385.

[8] R. M. Mohamed, M. M. Rashad, F. A. Haraz, W. Sigmund, Structure and magnetic properties of nanocrystalline cobalt ferrite powders synthesized using organic acid precursor method, J. Magn. Magn. Mater. 322 (2010) 2058.

[9] M. Sajjia, M. Oubaha, T. Prescott, A. G. Olabi, Development of cobalt ferrite powder preparation employing the sol-gel technique and its structural characterization, J. Alloys Compd. 506 (2010) 400.

[10] W.S. Chiu, S. Radiman, R. Abd-Shukor, M. H. Abdullah, P.S. Khiew,Tunable coercivity of CoFe2o4 nanoparticles via thermal annealing treatment, J. Alloys Compd. 459 (2008) 291.

[11] C. Inui, Y. Tsuge, H. Kura, S. Fujihara, S. Shiratori, T. Sato, Preparation of one- dimensional photonic crystals by sol–gel processfor magneto-optical materials, Thin Solid Films. 516 (2008) 2454.

[12] C.H. Yan, Z. G. Xu, F. X. Cheng, Z. M. Wng, L.D. Sum, C. S. Liao, J.T. Jia, Nanophased $CoFe_2O_4$ prepared by combustion method, Solid State Commun. 111 (1999) 287.

[13] X. Li, C. Kutal, Synthesis and characterization of superparamagnetic $Co_xFe_{3-x}O_4$ Nanoparticles, J. Alloys Compd. 349 (2003) 264.

[14] P.C .Rajath Varma, R. Sekhar Manna, D. Banerjee, M. Raama Varma, K. G. Suresh, A. K. Nigam, Magnetic properties of CoFe2O4 synthesized by solid state, citrateprecursor and polymerized complex methods: A comparative study, J. Alloys Compd. 453 (2008) 298.

[15] R. Sato Turtelli, Giap V. Duong, W. Nunes, R. Grossinger, M. Knobel, Magnetic properties of nanocrystalline CoFe2O4 synthesizedby modified citrate-gel method, J. Magn. Magn. Mater. 320 (2008) e339.

[16] Cabarias, M. Poliakoff, The continuous hydrothermal synthesis of nano-particle ferrites in near critical and supercritical water, J. Mater. Chem. 11 (2001) 1408.

[17] S. M. Montemayor, L. A. G. Cerda, J. R. T. Lubian, Preparation and characterization of cobalt ferrite by the polymerized complex method, Mater. Lett. 59 (2005) 1056.

[18] J. Ding, P. G. McCormick, R. Street, Magnetic properties of mechanically alloyed $CoFe_2O_4$, Sol. State Commun. 95 (1995) 31.

[19] R. Sani, A. Beitollahi, Yu. V. Maksimov, I. P. Suzdalev, Synthesis, phase formation study and magnetic properties of CoFe2O4 nanopowder prepared by mechanical milling, J. Mater. Sci. 42 (2007) 2126.

[20] Y. Shi, J. Ding, H. Yin, $CoFe_2O_4$ nanoparticles prepared by the mechanochemical method , J. Alloys. Compd. 308 (2000) 290.

[21]Y. Wan Ju, J. Hyun Park, H. Ryun Jung, S. June Cho, W. Jin Lee, Fabrication and characterization of cobalt ferrite (CoFe2O4) nanofibers by electrospinning, Mater. Sci. Eng. B147 (2008) 7.

[22] A.Y. Obaid, A. O. Alyoubi, A. A. Samarkandy, S. A. Al-Thabaiti, S. S. Al-Juaid, A. A. El-Bellihi , El- H. M. Deifallah,Kinetics of thermal decomposition of coper (II) acetate monohydrate, J. Therm.Anal. Calori. 61 (2000) 985.

[23] El-H. M. Diefallah, Kinetic analysis of thermal decomposition reactions:part VI. Thermal decompositionof manganese(II) acetate tetrahydrate, Thermochim. Acta. 202 (1992) 1.

[24] M. E. Brown, D. Dollimore ,A. K. Galwey, Comprehensive Chemical Kinetics, 22, Elsevier, Amsterdam 1980.

[25]M. E. Brown, Introduction to Thermal Analysis, Chapman and Hall, Chapter 13, 1988.

[26] D. Chen, X. Gao and D. Dollimore, Computer programs for kinetic analysis of non- isothermal TG data. Instrum Sci Tech, Analy. Instrumen. 20 (1992) 137.

[27] C. D. Doyle, Series Approximations to the Equation of Thermogravimetric Data, Nature 207 (1965) 290.

[28] J. Zsakó, Kinetic analysis of thermogravimetric data , J. Thermal Anal. 2 (1970) 145 .

[29] B. Carrol , E. P. Manche, Kinetic analysis of chemical reactions for non-isothermal Procedures, Thermochim. Acta. 3 (1972) 449.

[30] A. W. Coats , J. P. Redfern, Kinetic Parameters from Thermogravimetric Data, Nature 201 (1964) 68.

[31] T. Ozawa, A New Method of Analyzing Thermogravimetric Data, Bull. Chem. Soc. Jpn., 38 (1965) 1881.

[32] P. M. Madhusudanan, New approximation for the p(x) function in the evaluation of non- isothermal kinetic data, Thermochim.Acta. 97 (1986) 189.

[33] El-H. M. Diefallah, A. Y. Obaid, A. H. Qusti, A. A. El-Bellihi and M. Abdel Wahab, Gamma irradiation effects on the kinetics of the non-isothermal decomposition of manganese acetate tetrahydrate, Thermochim. Acta. 274 (1996)) 165.

[34] S. Guillemet-Fritsch, C. Chanel , J. Sarrias, S. Bayonne, A. Rousset, X. Alcobe, M. L. Martinez Sarriòn, Structure, thermal stability and electrical properties of zinc Manganites, Solid State Ionics, 128 (2000) 233 .

[35] H. P. Klug, L. E. Alexander, X-ray diffraction procedures for polycrystalline and amorphous materials, Wiley, New York, (1970).

[36] R. D. Waldron, Infrared Spectra of Ferrites, Phys. Rev. 99 (1955) 1727.

[37] S. N. Basahel, El-H. M. Diefallah, Kinetic Analysis of Thermal Decomposition Reactions.VII. Effect of Radiation and Doping on the Thermal Decomposition of BaCO3-TiO2 and SrCO3-TiO2 Crystalline Mixture, Can. J. Chem. 70(1992) 888.

[38] Z. A. Omran, M. A. Mousa, A. A. Abdel-Fattah, El-H.M. Diefallah, Kinetic analysis of thermal decomposition reactions - Part IV: Kinetics of formation of barium titanate in crystalline mixtures of barium carbonate and titanium dioxide, Thermochim. Acta. 145 (1989)271.

[39] T. Yamaguchi, S. H. Cho, H. Nagai , H. Kuno. Evaluation and Effects of Dispersion and Mixing Method of Reactant Particles on the Kinetics and Mechanism of Solid State Reactions, React. Solids Proc. Int. Symp. 8th.Plenum, New York. 1977.

[40] R.S. Devan, B.K. Chougule, Effect of composition on coupled electric, magnetic, and dielectric properties of two phase particulate magnetoelectric composite, J. Appl. Phys. 101 (2007) 014109 .

[41] R. P. Mahajan, K. K. Patankar, M. B. Kothale, S. A. Patil, Conductivity, dielectric behaviour and magnetoelectric effect in copper ferrite–barium titanate composites , Bull. Mater. Sci., 23 (2000)273.

[42] I. G. Austin, N. F. Mott, Polarons in crystalline and non-crystalline materials, Adv. Phys. 18 (1969) 41.

[43] K. K. Patankar, S. S. Joshi, B. K. Chougule, Dielectric Behaviour in Magnetoe-lectric Composites, Phys. Lett. A 346 (2005) 337.

[44] D. Alder, J. Fienleib, Electrical and Optical Proper- ties of Narrow-Band Materials, Phys. Rev. B 2 (1970) 3112.

[45] R.V. Mangalaraja, S. Ananthakumar, P. Manohar, F. D Gnanam, Magnetic, electrical and dielectric behaviour of Ni 0.8Zn 0.2Fe 2O 4 prepared through flash combustion technique, J. Magn. Magn. Mater. 253(2002) 56.

[46] D. Ravinder, K. V. Kumar, Dielectric behaviour of erbium substituted Mn–Zn ferrites, Bull. Mater. Sci. 24 (2001) 505.

[47] R. V. Mangalaraja, S. Anathakumar, P. Manohar, F. D. Gnanam, Magnetic, electrical And dielectric behaviour of Ni0.8Zn0.2Fe2O4 prepared through flash combustion technique , J. Magn. Magn. Mater. 253(2002)56.

[48] C.G. Koop, On the Dispersion of Resistivity and Dielectric Constant of Some Semiconductors at Audiofrequencies, Phys. Rev. 83(1951)121.

[49] M. Mallapur, P. A. Shaikh, R. C. Kambale, H. V. Jamadar, P. U. Mahamuni, B. K. Chougule, Structural and electrical properties of nanocrystalline cobalt substituted nickel zinc ferrite, J. Alloys Compds. 479(2009)797.

Table 1: XRD, TEM and FT-IR data of the $CoC_4H_4O_6$-Fe_2 $(C_4H_4O_6)_3$ mixture samples.

Method of Analysis		E_a K.J mole^{-1}	Log A min^{-1}
Composite *I*		41.8	3.28
Composite *II*		48.3	4.46
Madhusudanan method	β=5	30. 7	0.8
	10	25.8	0. 6
	15	18.0	0.1
	20	22.8	0.6
	Av.	24.3	0.5
Coats-Redfern method	β=5	30.3	3.7
	10	25.4	3.8
	15	17.7	3.9
	20	22.4	4.1
	Av.	24.0	3.9
Ozawa method	α=0.1	116.4	11.6
	0.2	106. 8	10.4
	0.3	100.5	9. 7
	0.4	92. 1	8. 8
	0.5	97. 5	9.3
	0.6	91.6	8.6
	0.7	91.8	8.5
	0.8	97.9	9.0
	0.9	96.1	8.6
	Av.	99.0	9.4

Table 2: Activation parameters of the thermal decomposition step of Iron tartrate calculated according to A_4 model.

Sample	D_{XRD} (nm)	D_{TEM} (nm)	Phase structure	FT-IR data	
				ν_1 (cm^{-1})	ν_2 (cm^{-1})
$CoFe_{250}$	30	46	Fe_2O_3 $C_4H_4CoO_6$	883 656	566
$CoFe_{450}$	35	15	Co_3O_4 Fe_2O_3	665	566, 446
$CoFe_{750}$	61	111	Co_3O_4 Co Fe_2O_4 Fe_2O_3	619	563, 421
$CoFe_{1050}$	49	52	$COFe_2O_4$	580	458, 438 422

Table 3: The values of Ea for $CoFe_{1050}$

sample	Temperature Range (K)	Ea (ev)		
		10KHZ	800KHZ	3 MHZ
$CoFe_{1050}$	305-448	0.01	0.02	0.03
	473-598	0.10	0.11	0.11

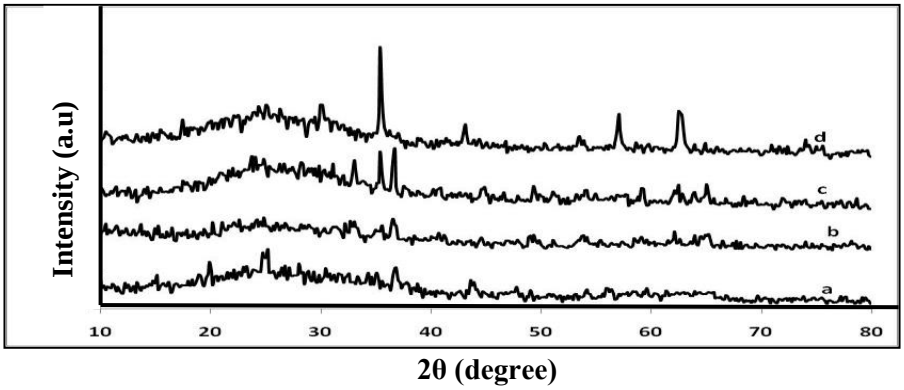

Fig.1: X-ray diffraction patterns for $CoC_4H_4O_6$–$Fe_2(C_4H_4O_6)_3$ mixture after being calcined at various temperatures (A=250 , b=450 , c=750 , d=1050°C).

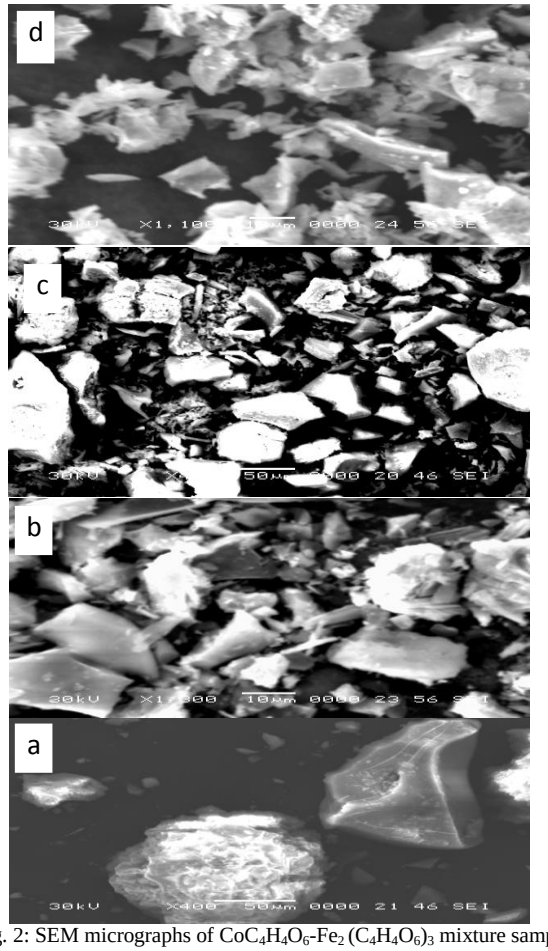

Fig. 2: SEM micrographs of $CoC_4H_4O_6$-$Fe_2(C_4H_4O_6)_3$ mixture samples heated at: a) 60 ºC b) 450 ºC c) 750 ºC d) 1050 ºC

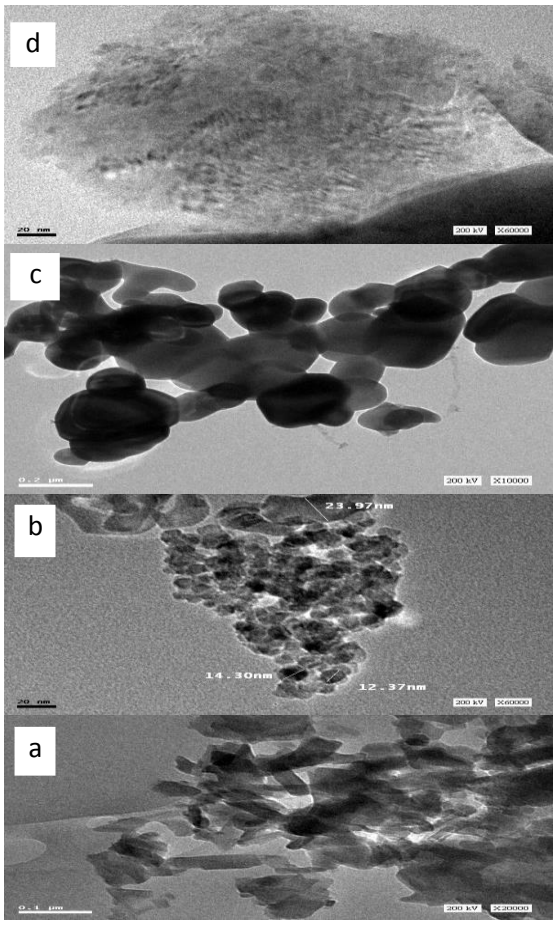

Fig. 3: TEM micrographs of $CoC_4H_4O_6$-Fe_2 $(C_4H_4O_6)_3$ mixture samples heated at: a) 60 °C b) 450 °C c) 750 °C d) 1050 °C

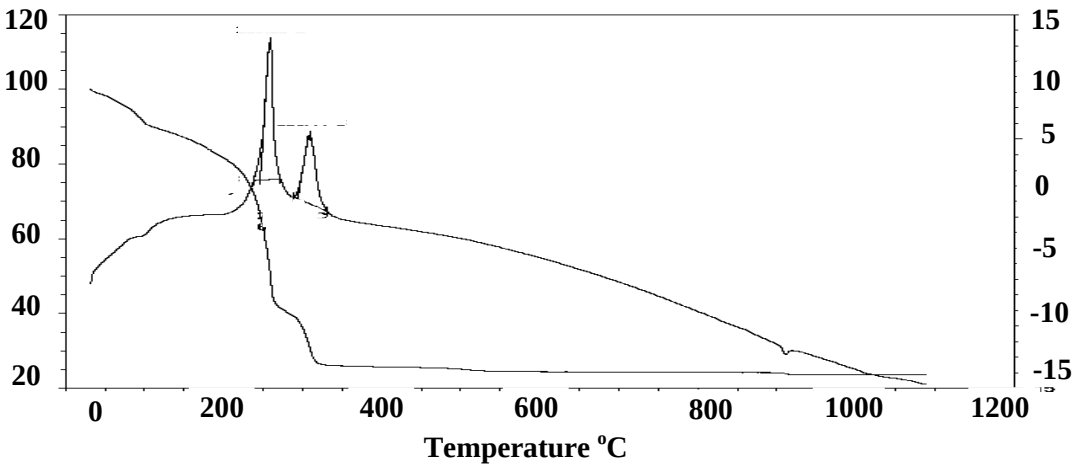

Fig. 4: DSC-TGA curves of $CoC_4H_4O_6$-Fe_2 $(C_4H_4O_6)_3$ mixture.

Heating rate=$10^{o}Cmin^{-1}$.

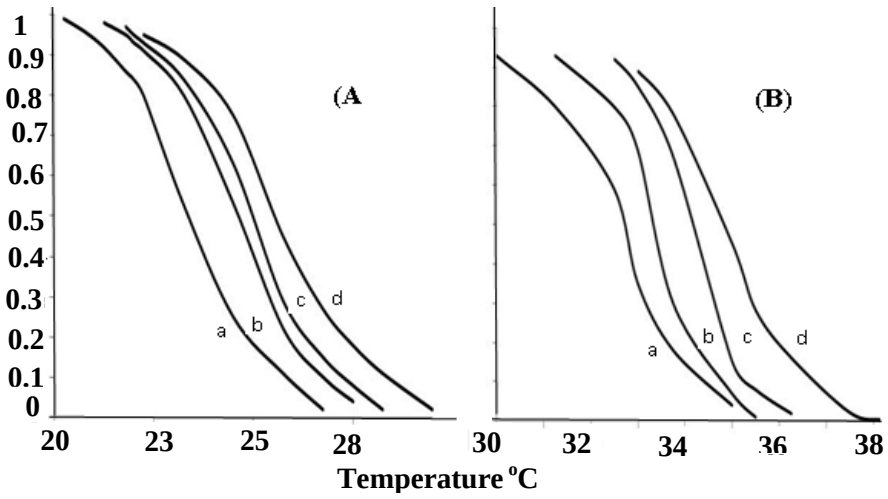

Fig 5: Dynamic measurents of thermal decomposition for $CoC_4H_4O_6$ –$Fe_2(C_4H_4O_6)_3$ mixture. Heating rates (β),a,5°Cmin^{-1}; b,10°Cmin^{-1}; c,15°Cmin^{-1}; d,20°Cmin^{-1} .(A)first decomposition step (B)second decomposition step .

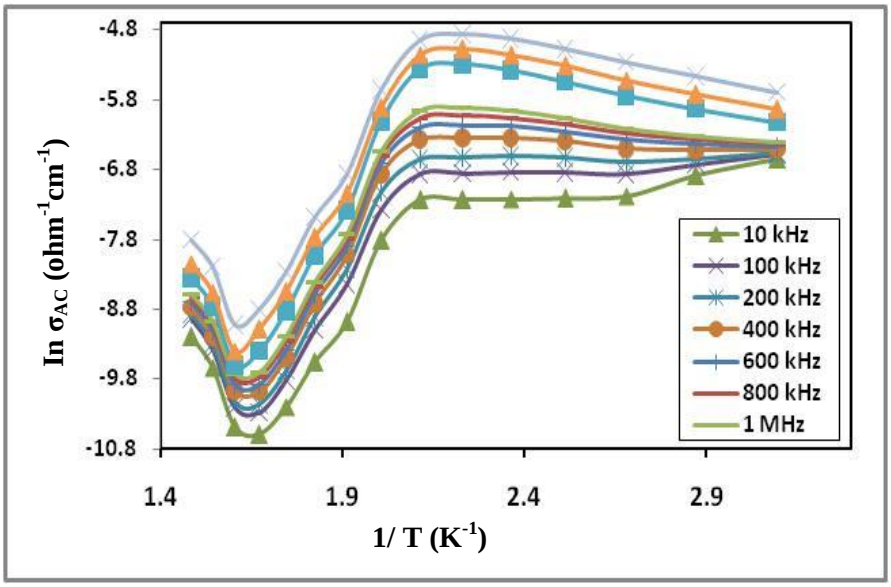

Fig 6: The temperature dependence of AC conductivity of $CoFe_2O_4$.

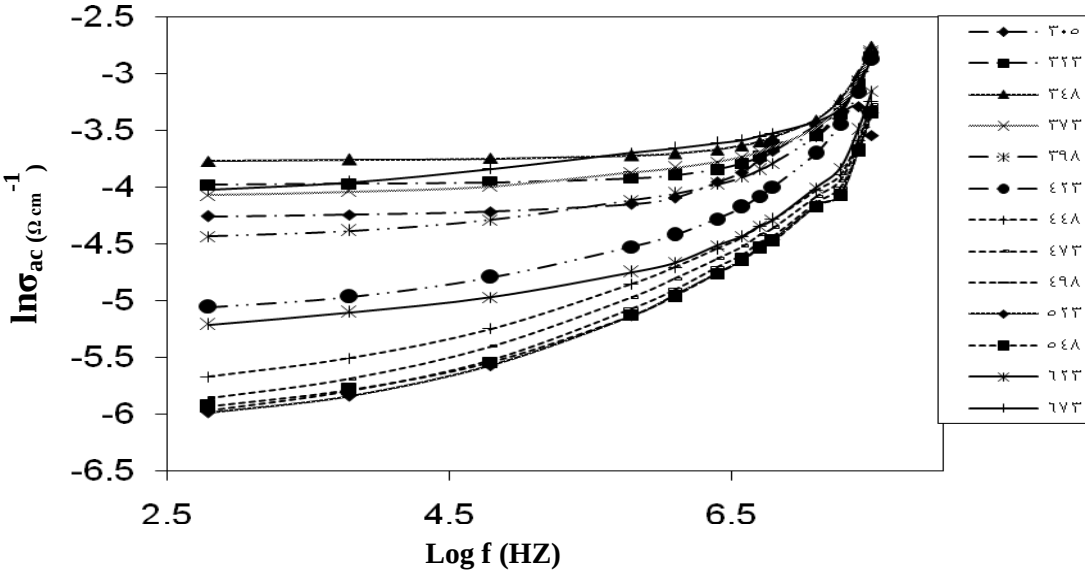

Fig. 7: Variation of ac conductivity (σ_{ac}) as a function of frequency is represented in

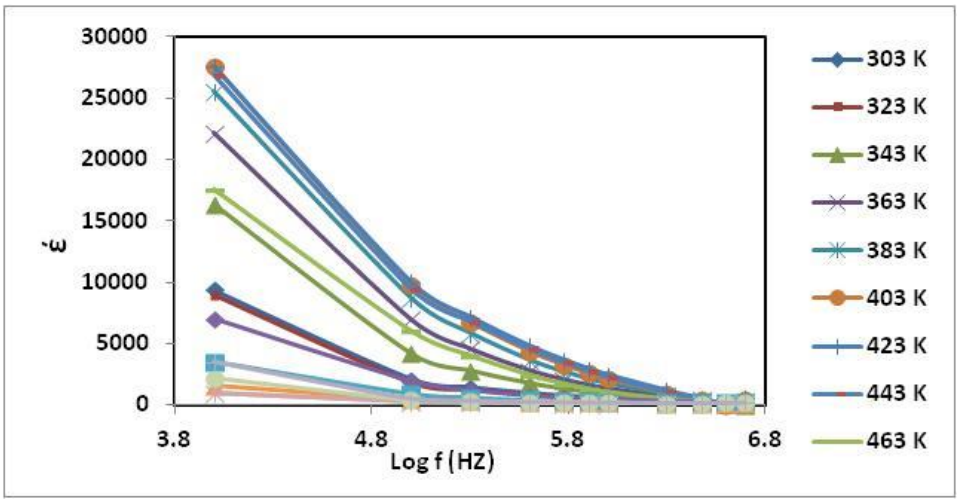

Fig. 8: the variation of the dielectric constant (ε`) with the absolute temperature as a function of frequency.

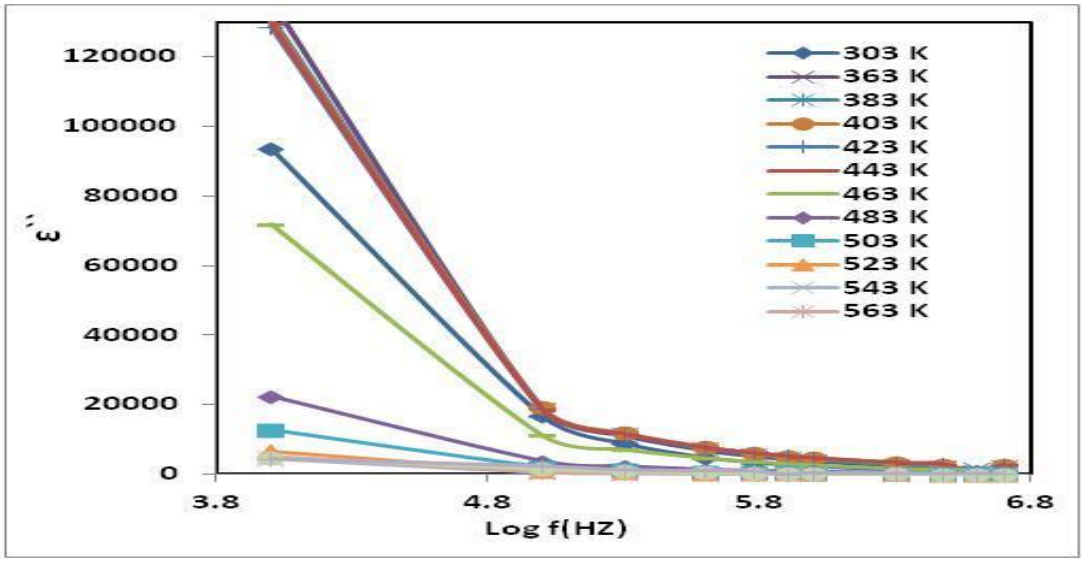

Fig. 9: The variation of dielectric loss for the sample annealed at various temperatures as a function of frequency is shown in.